Received: 4 September 2020 | Revised: 3 November 2020 | Accepted: 21 November 2020

DOI: 10.1002/er.6260

RESEARCH ARTICLE

INTERNATIONAL JOURNAL OF ENERGY RESEARCH WILEY

Hybrid heat sinks for thermal management of passively cooled battery chargers

Gurpreet Singh Sodhi[1,2] | **Chris Botting**[3] | **Eric Lau**[3] | **Muthukumar Palanisamy**[2] | **Mina Rouhani**[1] | **Majid Bahrami**[1]

[1]Laboratory for Alternative Energy Conversion (LAEC), School of Mechatronic Systems Engineering, Simon Fraser University (SFU), Surrey, British Columbia, Canada

[2]Department of Mechanical Engineering, Indian Institute of Technology Guwahati, Guwahati, India

[3]Delta-Q Technologies, Burnaby, British Columbia, Canada

Correspondence
Muthukumar Palanisamy, Department of Mechanical Engineering, Indian Institute of Technology Guwahati, Guwahati, Assam 781039, India.
Email: pmkumar@iitg.ac.in

Majid Bahrami, Laboratory for Alternative Energy Conversion (LAEC), School of Mechatronic Systems Engineering, Simon Fraser University (SFU), Surrey, BC V3T 0A3, Canada.
Email: mbahrami@sfu.ca

Funding information
The Canadian Queen Elizabeth II Diamond Jubilee Scholarships; SSHRC; IDRC

Summary

Battery chargers are an important component in electric and plug-in hybrid vehicles and various other clean energy systems. The thermal management in battery charger is a crucial aspect that influences its overall performance and cyclic stability. Passive cooling technology using heat sinks is preferred in developing battery chargers due to its reliability, quietness, and efficiency (no parasitic power). In the present work, new hybrid passive heat sinks (HPHS) with various fin geometries, namely inclined interrupted fins, pin fins, and straight interrupted fins, have been developed by adding a phase change material (PCM) layer to passively cooled bare fin heat sinks (BFHS). The developed heat sinks have the same geometric footprint as that of the battery charger, IC650 built by the industrial partner of the project Delta-Q Technologies. Experimental investigations were carried out to analyze the effects of PCM quantities and continuous (80-120 W) and intermittent (duty cycle operation) thermal loads on the heating-cooling performance of the HPHS. Temperature contours obtained using infrared images show that the proposed HPHS provides a more uniform temperature with reduced hot spots compared to BFHS. The heating and cooling performances of straight interrupted fins-based HPHS were found better for all thermal loads and PCM quantities tested due to their smaller thermal resistance. Increasing the PCM volume fraction from 0.2 to 0.6 improves the load shedding capacity. However, the added thermal resistance requires optimal consideration. While conducting different cyclic operations for inclined interrupted fins-based HPHS, a maximum overall thermal management ratio of 0.45 was achieved. The proposed HPHS minimizes the temperature fluctuations more effectively while operating at high loads and shorter duty periods. This new passively cooled hybrid heat sink can notably improve the overall performance and reliability of battery chargers during both continuous and intermittent operations.

KEYWORDS

battery charger, hybrid heat sink, passive cooling, phase change material, thermal management

1 | INTRODUCTION

Electric vehicle (EV) and plug-in hybrid vehicle markets are making rapid developments to cut the reliance on fossil fuels with a projected reduction of 127 million tonnes of oil equivalent by 2030.[1] A growth rate of 15% in EV demands is expected in the next decade.[2] This necessitates technological advances in electric powertrain engineering and improvement in the charging infrastructure. It is worth mentioning that the battery charging facilities need comprehensive enhancements, such as rapid charging rates to address the projected rise in EVs. The classical Moore's law forecasts the current increasing trend of electronic chip performances with increasing transistor density and reduction of size.[3,4] Due to the miniaturization of components, the failure rate of electronic devices increases exponentially because of thermal stress.[5] The significance of thermal management technology reflects on its growing market which is projected to increase from $12.4 billion in 2018 to $16.3 billion by 2023.[6] Therefore, efficient, reliable cooling is one of the foremost concerns to be addressed in power-electronic devices including battery chargers.

Significant research works have been carried out using different active/passive cooling technologies, namely heat-pipe-assisted cooling,[7,8] thermoelectric cooling,[9] cooling using microchannels,[10,11] and the use of thermal conductivity enhancers, such as fins.[12] The success of these methods is dependent on the size of the device, cost-effectiveness, reliability, availability of technology, and ergonomics of the design. Passive cooling technologies are widely preferred due to zero parasitic power consumption, noise-free operation, and higher reliability compared to active cooling technologies.[13] Electronic cooling has evolved significantly by incorporating thermal energy storage, which is instrumental in the effective thermal management of devices. Phase change materials (PCMs) used for this purpose function as an energy storage buffer and assist in "peak shaving" of the device load during phase change. PCMs have had a remarkable impact especially on the battery thermal management system (BTMS) in thermal load shedding.[14,15] PCMs control the temperature peaks and maintain uniform temperature in batteries provided that the selection of the melting temperature of PCM is appropriate.[16] Paraffins are most suitable for thermal management applications with a melting temperature range between 25°C and 85°C but suffer from a low thermal conductivity of ~0.1 to 0.4 W/m/K.[17] Adding thermally conductive materials, such as expanded graphite,[18] multiwalled carbon nanotubes,[19] graphene nanoplates,[20] and using copper foam,[21] improve the heat transfer characteristics of the PCM, but these additives compromise the volumetric energy storage density and the cost of the cooling system. In some cases, increasing the volume fraction of additives hampers the natural convection flow of the PCM due to a drastic rise in the liquid phase viscosity.[22] Thermal conductivity enhancers such as fins have low thermal resistance and act as a prime heat transfer interface between the device and PCM or the environment.

The proposed hybrid passive heat sinks (HPHS) offer a combination of existing heat sink topology with integrated PCM to act as a buffer for peak load shaving. The selection of PCM is based on properties such as melting temperature and energy storage density suitable for the application, whereas fin topology needs careful optimization. Our team at Simon Fraser University (SFU) has made notable contributions to the design and optimization of heat sink topology for passively cooled systems.[23,24] In addition to the heat sink design, a successful HPHS needs to be compatible with the applications. Battery charging technology, which is the focus of the present study, faces intricate challenges to develop reliable, efficient, and affordable devices. The key considerations include: (a) peak shaving of the operating load as the battery chargers start to de-rate at elevated temperatures and (b) intermittent operation with frequent power ON/OFF cycles. Hence, the proposed HPHS is a great candidate for thermal management requirements of battery chargers. The fin topology plays an important role in the heat transfer characteristics of a heat sink–based battery charger. A summary of HPHS studied in the literature which used fins as thermal conductivity enhancers is listed in Table 1.

Three different types of PCM heat sink configurations have been investigated. Firstly, employing PCM cavities on microprocessor chips, which have an inherent disadvantage due to low thermal conductivity of PCMs and, hence, low heat dissipation rate. Such designs are beneficial only if high thermal conductivity additives such as expanded graphite[33] and graphene[20] are added to the PCM. Zarma et al[34] studied series and parallel arrangements of multicavity heat sink filled with nanoparticle-enhanced PCM to control the temperature of a concentrator photovoltaic (CPV) system. They concluded that parallel multicavity arrangement provided higher heat dissipation rate due to better contact of the metal surfaces with the CPV heat transfer surfaces. In the second design, fins submerged in PCMs are used as thermal conductivity enhancers to improve the heat transfer characteristics of the PCM enclosed in containers. Most of the studies presented in Table 1 have used this design and investigated the effect of fin characteristics such as geometry, fin volume to PCM volume ratio, and material[25-27,30,31] on the heat sink

TABLE 1 Summary of literature on HPHS using fins as thermal conductivity enhancers

References	Key findings/notes
Ali et al[25]	• Comparison of square and cylindrical pin fin geometries for equal fin volume. • Cylindrical pin fins showed better thermal management.
Ali et al[26]	• Triangular fins as better fin designs than cylindrical and rectangular fins.
Ali and Arshad[27]	• Studied the impact of fin thickness on HPHS performance. • Best thermal conductance was achieved for an optimum fin thickness (3 mm).
Mahmoud et al[28]	• Developed low-weight and low-cost honeycomb inserts as a replacement of machined fins.
Fok et al[29]	• Investigated the effect of the number of fins and heat sink orientation. • Increasing the number of fins improved the performance, whereas the impact of orientation was negligible.
Baby and Balaji[30]	• Study of pin fin and plate fin geometries and defining a modified Stefan (Ste*) number as a basis for performance comparison. • Lower Ste* and better performance enhancement for pin fins were observed.
Baby and Balaji[31]	• Proposed a genetic algorithm to optimize hybrid pin fin heat sink topology.
Jaworski[32]	• Developed a novel open-air active cooling design with pipe fins filled with PCM to improve heat transfer rate as compared to a system with simple PCM containers.

performance. Due to no interaction of fins with the ambient, heat dissipation rate of such heat sinks is significantly low, especially during the device non-operation (OFF). This leads to slow restoration of the system before the start of the next operational cycle. Akula et al[35] proposed a heat sink design strategy with horizontal fins known as baffles submerged in the PCM to enhance the heat sink cooling rate. They investigated the effects of PCM filling amount and heat sink orientation on the discharging (device OFF mode) time. The baffles led to the creation of cold spots, thus improving the cooling rate significantly. The third and the least studied design is the PCM-air hybrid heat sink design, which combines the effect of fin interaction with the PCM and the ambient.[28,32,36] This design facilitates continuous heat dissipation from the heat sink to the ambient via natural or forced convection heat transfer.[17,37] Additionally, the fin topology impacts the overall heating-cooling (ON/OFF) operation of the device. Ghanbarpour et al[38] numerically analyzed plate-fin hybrid heat sinks combined with a heat pipe. They observed a significant reduction in the maximum heat sink temperature, which was mainly influenced by the heat transfer dissipation capacity of the fins exposed to the ambient air. In spite of several benchmark studies discussing the impact of PCM on fin-based heat sinks, their applications are limited to basic shapes such as pin fins or plate fins.

Based on the literature review, the following gaps in the literature are required to be addressed in order to develop HPHS for battery chargers:

- Only a few studies have discussed about the performances of HPHS during intermittent operation.[39-42]
- The reported HPHS prototypes were focused on portable/small-scale applications with a device thermal load of ~1 W to 40 W.[19,29]
- Lack of an investigation on the performance of HPHS featuring fin geometries developed for real industrial applications.[43,44]
- Very few researchers have studied the influence of varying the PCM quantity on the performance enhancements in HPHS during the complete heating-cooling operation.[35]

In the present study, a detailed experimental analysis has been performed on HPHS considering the above-mentioned research gaps. To the best of the authors knowledge, the analysis of hybrid heat sinks incorporating fins partially submerged in the PCM for an effective passive cooling mechanism has not been presented previously. The objective of the present study is to develop a new HPHS, where a PCM layer is added to the bare fin heat sinks (BFHS) of a battery charger to extend its operation at peak load. The performance of three HPHS designs with various fin geometries, including: (a) inclined interrupted fins; (b) pin fins; and (c) straight interrupted fins were analyzed through experimental investigations. The heat sinks have the same footprint as the IC650 battery chargers developed by Delta-Q Technologies,[44] shown in Figure 1. The IC650 delivers a rated power of 650 W at a thermal load between 85 W and 95 W and is used in electric pallet jacks, floor care machines, scissor lifts, and e-mobility scooters. The performance of the heat sinks was analyzed by varying several parameters, such as heat sink thermal load and PCM quantity. Infrared images were taken to elaborate the thermal distribution during the heating cycle and compare the hot spots developed in heat sinks with and without the PCM layer. The impact of intermittent duty-cycle operation on the temperature control and overall thermal management ratio (TMR) using HPHS was also analyzed.

FIGURE 1 An IC650 industrial battery charger developed by Delta-Q Technologies[44] [Colour figure can be viewed at wileyonlinelibrary.com]

2 | EXPERIMENTAL STUDY

A custom-built testbed was designed and fabricated in our lab at SFU to study the performance of HPHS. The major components of the testbed are shown in Figure 2A. The heat sinks were subjected to a thermal load using an electric heater and power source, which was a programmable DC output (Chroma 62012P-100-50) and capable of generating thermal power in the range between 20 W and 120 W. Figure 2B shows the exploded view of the HPHS assembly. A polyimide heater (with an electrically insulated KAPTON film) that was 100 mm × 150 mm in size was attached to the base of the heat sink to mimic the heat generated by a battery charger during operation. The heater was attached using a thermal interface material to minimize the thermal contact resistance between the heater and the heat sink. The heat sinks were installed in a plexiglass container, which contains the PCM. Temperatures were measured using T-type thermocouples (copper-constantan, accuracy ±1°C) at various locations: six at the heat sink base as shown in Figure 2C, six at the fin tip at the same location as the base and six distributed within the PCM to determine hot spots and temperature distribution. A data acquisition system (National Instruments cDAQ-9174) was used to record temperature and voltage measurements. Module NI-9229 and NI- 9212 were used as a voltage analog input unit and temperature acquisition modules, respectively. The complete flow process of the system was monitored by an in-house LabVIEW code. Additionally, an infrared camera (Flir i7) was used to capture the infrared images as a record of thermal distribution during the tests. In the experimental analysis, the average temperatures of the thermocouples fixed at the heat sink base and within the PCM were considered. The experiments were stopped when the change in the average base temperature dropped below 0.5°C and the steady state was achieved.

The key performance indicator to evaluate the HPHS performance is the time delay in the heat sink operation at temperatures lower than peak temperatures.[25-27,30] The PCM selected for the HPHS in the present study is intended to extend the isothermal battery charger operation near the melting point temperature and absorbing the latent heat completely. Hence, the enhancement factor (ε) is introduced as the ratio of time taken by the HPHS to the time taken by the BFHS to reach the PCM melting temperature during heating as shown in Equation (1).

$$\varepsilon = \frac{t_{\mathrm{HPHS}}}{t_{\mathrm{BFHS}}}. \tag{1}$$

Figure 3 shows the thermal resistance network of the HPHS with fins partially submerged in the PCM. The heat transfer from the device to the environment depends upon various intermediate thermal resistances, including thermal contact resistance at the heat sink base, fins and PCM thermal resistances, and the ambient convection and radiation thermal resistances. The overall thermal performance of different HPHS samples loaded with different PCM quantities is calculated based on the thermal conductance (G) given in Equation (2). The parameter G has been previously analyzed by different researchers, including Ali et al[25,27,45] and Gharbi et al[46] to compare the performance of different heat sink configurations.

$$G = \frac{P}{T_{\max} - T_a}, \tag{2}$$

where $T_{\max}$ and T_a are the maximum heat sink temperature and the ambient temperature during heating and P is the input power.

Uncertainties in the present data set exist due to the uncertainties in the measured DC voltage, current, and temperature. The accuracy of T-type thermocouples used for measurement of temperature is ±1°C. As per the specifications given by the National Instruments, the maximum error of the voltage acquisition modules is ±1.2%. The maximum uncertainty is determined using the Kline and McClintock method,[47] as shown in Equation (3).

$$X_s = \left(\sum \left(\frac{\partial Z}{\partial Y_i} \delta Y_i \right)^2 \right)^{1/2}. \tag{3}$$

where X_s is the uncertainty associated with Z (y_1, y_2, y_3, ...y_n) and the uncertainty of independent variables Y_i is

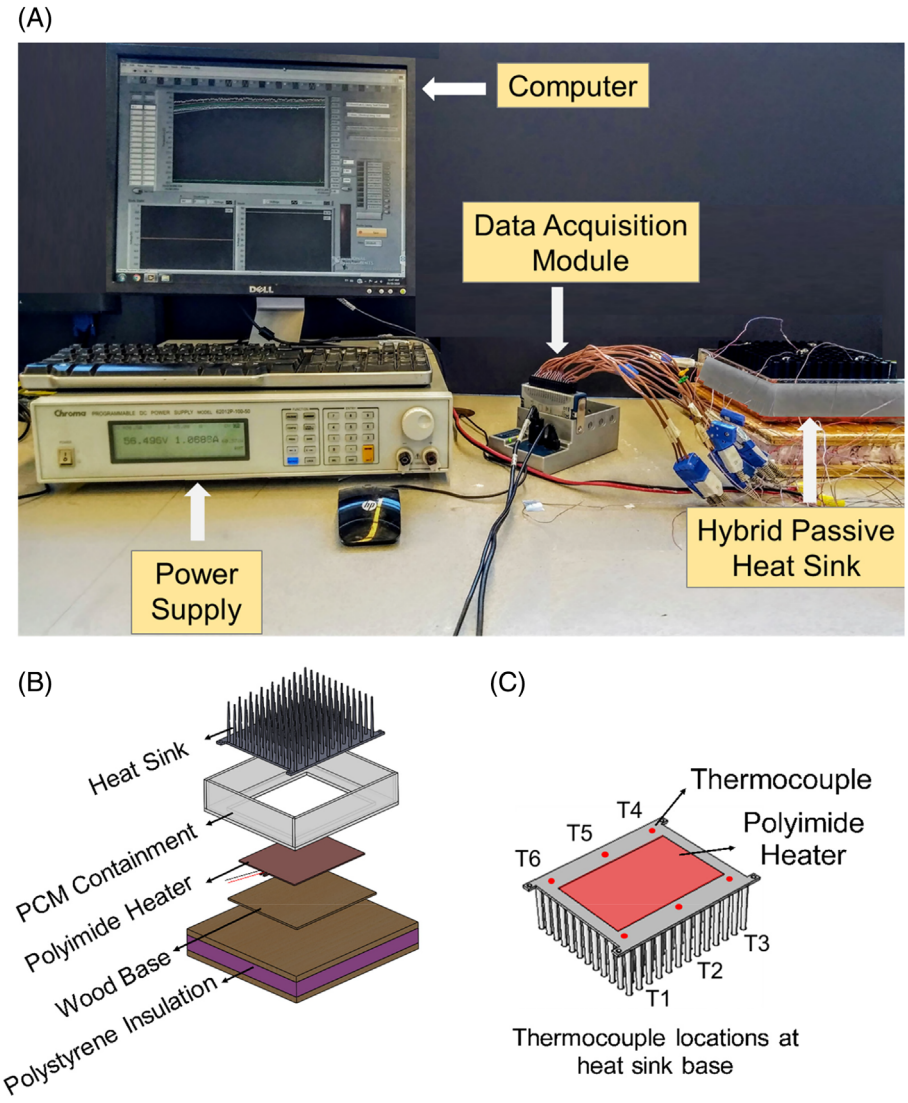

FIGURE 2 Schematic of the testbed: (A) custom-built setup to test the heat sink performance; (B) exploded view of hybrid passive heat sink (HPHS) assembly; and (C) location of thermocouples installed at the heat sink base [Colour figure can be viewed at wileyonlinelibrary.com]

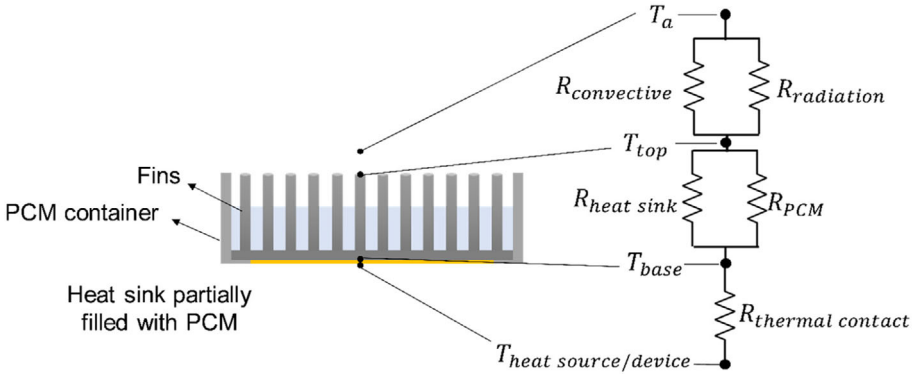

FIGURE 3 Thermal resistance network for the hybrid passive heat sink [Colour figure can be viewed at wileyonlinelibrary.com]

X_i. The uncertainty in input power (Equation (4)) is estimated as ±1.7%.

$$\frac{\delta P}{P} = \left(\left(\frac{\delta V}{V} \right)^2 + \left(\frac{\delta I}{I} \right)^2 \right)^{\frac{1}{2}}. \quad (4)$$

2.1 | Heat sink samples

The heat sink samples were fabricated using Computer Numerical Control (CNC) machining from Aluminum alloy 6061-T6 at SFU's in-house machine shop. To enhance the radiation heat transfer of fins, the surfaces were

anodized which led to a notable increase in surface emissivity from 0.03 to 0.89.[43] The schematic showing the heat sink samples (non-anodized) and dimensions with different fin geometries is shown in Figure 4. The size of the base for all the heat sinks is 160 mm (L) × 180 mm (W) and the height (H) is 60 mm. The sample names and dimensions are described in Table 2. The design of the inclined interrupted fins is inspired by the benchmark product, IC650 battery charger developed by Delta-Q Technologies. The heat sink geometries with inclined fins and interrupted fins developed in the present study have been scarcely reported in the literature. Fujii[48] studied the impact of inclination angle of fins on the heat transfer characteristics of vertically placed heat sinks and found that inclining the fins improves the heat transfer rate as it leads to interruption of thermal boundary layers. Ahmadi et al[24] discussed the concept of thermal boundary layer interruption in a continuous straight fins-based heat sink. As reported extensively in the literature, the circular pin fins designs reduce the heat sink thermal resistance significantly.[49]

The prototyping of the heat sinks and their testing at different orientations were already performed by the author's research team. The performance of the actual industrial heat sink has been reported by Zhang et al,[43,50] and it was confirmed from their study that the heat sinks mimic the battery charger operation under identical ambient conditions. As previously mentioned, the overall geometric footprint of all the heat sinks is same as that of IC650 battery charger. The heat transfer surface area of all the heat sinks is approximately the same (~0.25-0.26 m^2) with a maximum relative difference of ±1.25%.

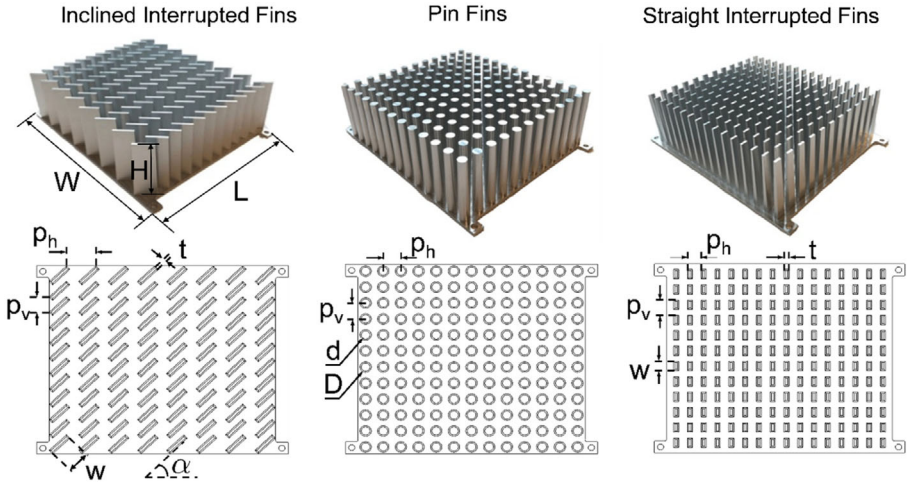

FIGURE 4 Heat sink samples and the top view of different fin geometries: inclined interrupted fins, pin fins, and straight interrupted fins [Colour figure can be viewed at wileyonlinelibrary.com]

TABLE 2 Heat sink samples and their dimensions

	Inclined interrupted fins	Pin fins	Straight interrupted fins
Heat sink sample type			
Heat sink without a PCM layer	BFHS1	BFHS2	BFHS3
Heat sink with a PCM layer	HPHS1	HPHS2	HPHS3
Geometrical parameter			
Vertical fin pitch (p_v) [mm]	9.5	13.7	13
Horizontal fin pitch (p_h) [mm]	23	14.2	10.9
Fin thickness (t)/diameter (D) at base [mm]	3.9	9	3.9
Fin thickness (v)/diameter (d) at top [mm]	1.8	6.9	1.8
Fin width (w) [mm]	19	—	8
Horizontal fin inclination (α) [°]	44	—	—
Heat sink length (L) [mm]	180	180	180
Heat sink width (W) [mm]	160	160	160
Number of fins per column (n)	12	12	12
Number of columns (N)	8	13	16

2.2 | Phase change material

A commercial-grade paraffin wax (PCM 58, Microtek Laboratories Inc.) was used as the PCM in HPHS designs. The selection is based on the desired isothermal phase change temperature range of the PCM suitable for the device operation. PCM 58 has a thermal conductivity of 0.3 W/m K, measured using a transient plane source (TPS 2500S, ThermTest Inc., Canada) technique with a Kapton C7577 sensor at our lab.[51] Repeated measurements (10-12 measurements) were taken, and the uncertainty of the measured thermal conductivity was calculated as ±0.028 W/m/K. The latent heat of the PCM was measured using a differential scanning calorimetry (DSC) analyzer (DSC 6000, Perkin Elmer). The heating-cooling DSC curve is plotted in Figure 5. The PCM melting point temperature from the DSC analysis was found to be 58.3°C, and the calculated melting and solidification phase change enthalpies were 146.1 and 145.3 J/g, respectively. The volume fraction of the PCM is calculated as the ratio of the liquid PCM volume used to the total heat sink volume (160 mm × 200 mm × 60 mm) using Equation (5).

$$\phi = \frac{V_{\text{PCM}}}{V_{\text{total}}}. \tag{5}$$

Adding PCM to different volume fractions always leaves fins partially exposed to the ambient to facilitate the heat transfer to the ambient. A maximum difference of ~2 mm in the PCM layer height was observed between different HPHS due to different volumes of fin geometries; however, the effects due to the marginal change in height were neglected.

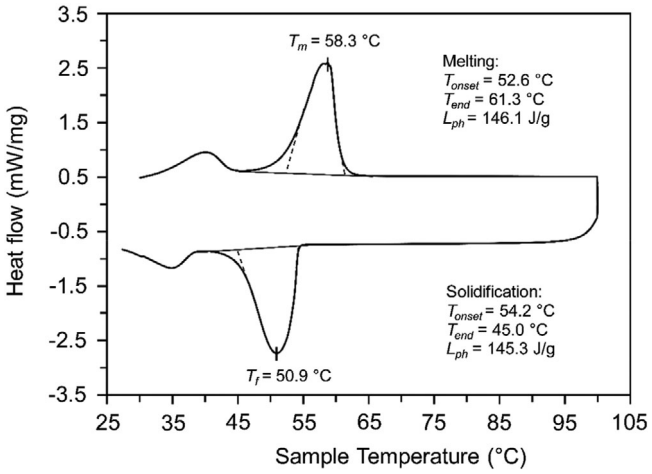

FIGURE 5 Differential scanning calorimetry curve for melting and solidification of PCM 58

3 | RESULTS AND DISCUSSION

3.1 | HPHS operation

The average PCM temperature profile of HPHS1 with a PCM volume fraction of 0.4 (m_{PCM} = 585 g) at a thermal load of 80 W during a complete heating-cooling cycle is shown in Figure 6. During the device operation (ON mode), the device generates heat which is transferred from the base to the fins and the PCM. For a specified volume fraction, the fins were partially submerged in the PCM up to half of their height ($H/2$) and partially exposed to the ambient. The heat is rejected continuously to the ambient from the exposed fin surfaces. Initially, the PCM undergoes sensible heating process (process ab), followed by its melting (process bc) in the temperature range of 52°C to 61°C based on our DSC study of PCM 58 as shown in Figure 5. As the PCM changes phase from solid to liquid, it stores a significant amount of latent heat. During this period, the heat sink temperature is maintained near the PCM melting temperature for a prolonged period due to the isothermal behavior of the phase change process. This process is followed by sensible heating of the liquid PCM (process cd) during which the PCM temperature starts rising gradually until it reaches a steady-state temperature (T_s) of ~79°C, which depends, in part, on the heat rejection capacity of the bare area of the fins. The HPHS serves a dual purpose during the ON mode: (a) continuous heat loss to the ambient through the active fin volume exposed to the ambient and (b) latent heat stored in the PCM. PCM heat storage improves the peak load shaving capacity of the device and controls the temperature at the device level near the melting temperature of the PCM during the phase change.

During the cooling (OFF mode), the PCM undergoes discharging, and the heat stored in the PCM is

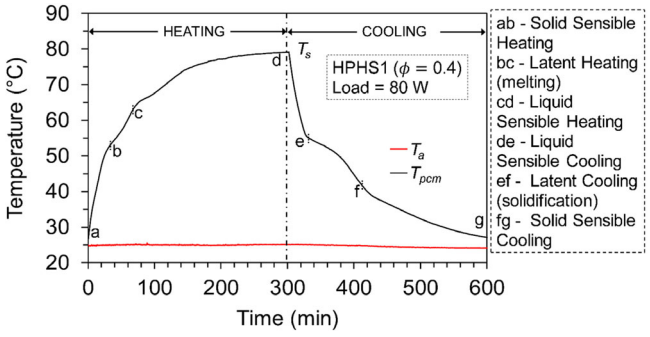

FIGURE 6 Sequence of processes during the heating-cooling cycle for hybrid passive heat sink (HPHS) with a PCM volume fraction of 0.4 (m_{PCM} = 585 g) at a thermal load of 80 W [Colour figure can be viewed at wileyonlinelibrary.com]

transferred to the ambient due to the temperature difference between the heat sink and the ambient. The cooling process starts with the sensible cooling of liquid PCM (process de), followed by its solidification (process ef) and cooling of solid PCM (process fg), as illustrated in Figure 6.

3.2 | Effect of hybridization on heat sink performance

Figure 7 shows the base temperature profile for BFHS1 and HPHS1 at a thermal load of 80 W and PCM volume fraction of 0.4. It is observed that HPHS1 provides a time delay in heat sink thermal response throughout the heating process. The base temperature of HPHS1 reached the PCM melting temperature (T_m) in 56 minutes, that is, took 42 minutes more than BFHS1, and the calculated enhancement factor (ε) is 4. The steady-state temperature of BFHS1 was 71°C, and to attain this temperature, the HPHS1 operation delayed by 53 minutes, that is, 74% more than BFHS1. HPHS1 extended the heat sink operation until the PCM melted completely, however, during the sensible heating of liquid PCM, the HPHS1 temperature started increasing again and reached a steady-state condition at 78°C in another 100 minutes. This indicates effective temperature control offered by the proposed HPHS during the heat sink loading.

While performing tests on HPHS2 and HPHS3, the delay in time to reach T_m for HPHS2 (than BFHS2) was 170% ($\varepsilon = 2.7$), and the delay for HPHS3 (than BFHS3) was 260% ($\varepsilon = 3.6$). It is to be noted that the steady-state temperatures of all HPHS were higher than the corresponding BFHS by 5°C to 8°C. Therefore, even though the HPHS provide effective temperature control and load peak shaving during the PCM melting, the liquid sensible heating profile and the time to reach steady state are critical factors in deciding the degree of hybridization required. The benefits due to hybridization are subjected to conditions, such as the PCM quantity and optimum duty-cycle operation discussed later in the study.

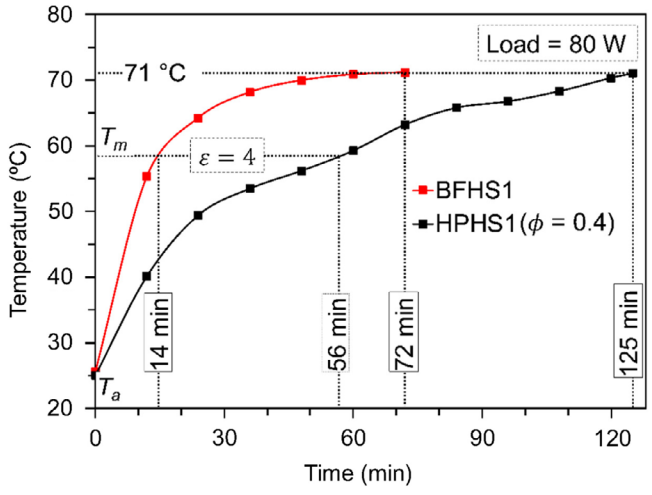

FIGURE 7 Variation in the base temperature profiles for BFHS1 and HPHS1 with PCM volume fraction of 0.4 at a thermal load of 80 W [Colour figure can be viewed at wileyonlinelibrary.com]

3.2.1 | Hot spot evaluation

During heat sink testing, the hot spots were formed at the center of BFHS and HPHS. Figure 8 shows the hot spot temperatures of BFHS3 and HPHS3 with a PCM volume fraction of 0.4 and a thermal load of 80 W at different time intervals. The hot spot temperature of BFHS3 had risen to 66.3°C in 30 minutes, whereas the hot spot temperature of HPHS3 was ~20°C cooler than BFHS3 at this time interval. It can be inferred that the BFHS experiences a high rise in temperature instantly during the heating process, whereas the HPHS, on the other hand, delays the temperature rise and maintains the device at a lower temperature for a longer period. The hot spot temperature difference between the BFHS and the HPHS after 50 minutes was ~14.5°C. BFHS3 reached a steady-state temperature of 76.5°C after 70 minutes of operation. The hot spot temperatures of HPHS3 were still cooler by ~10°C at 70 minutes and by ~5°C at 90 minutes. The ability of the HPHS to store energy as latent heat helps in sustaining high thermal loads without sudden temperature rise, whereas the BFHS cannot sustain such loads and as a result, the bulk temperature of the system increases. It should also be noted that employing HPHS also leads to an almost uniform heat sink temperature throughout its surface.

3.3 | Comparison of different HPHS samples

3.3.1 | Heating process

The base temperature profiles for a thermal load of 80 W and a PCM volume fraction of 0.4 of HPHS (HPHS1, HPHS2, and HPHS3) are shown in Figure 9. It is observed that the temperature profiles are similar up to 65°C, and the times taken by all the HPHS to reach this temperature are nearly the same, that is, 80 minutes, 76 minutes, and 75 minutes for HPHS1, HPHS2, and HPHS3, respectively. The PCM undergoes sensible and

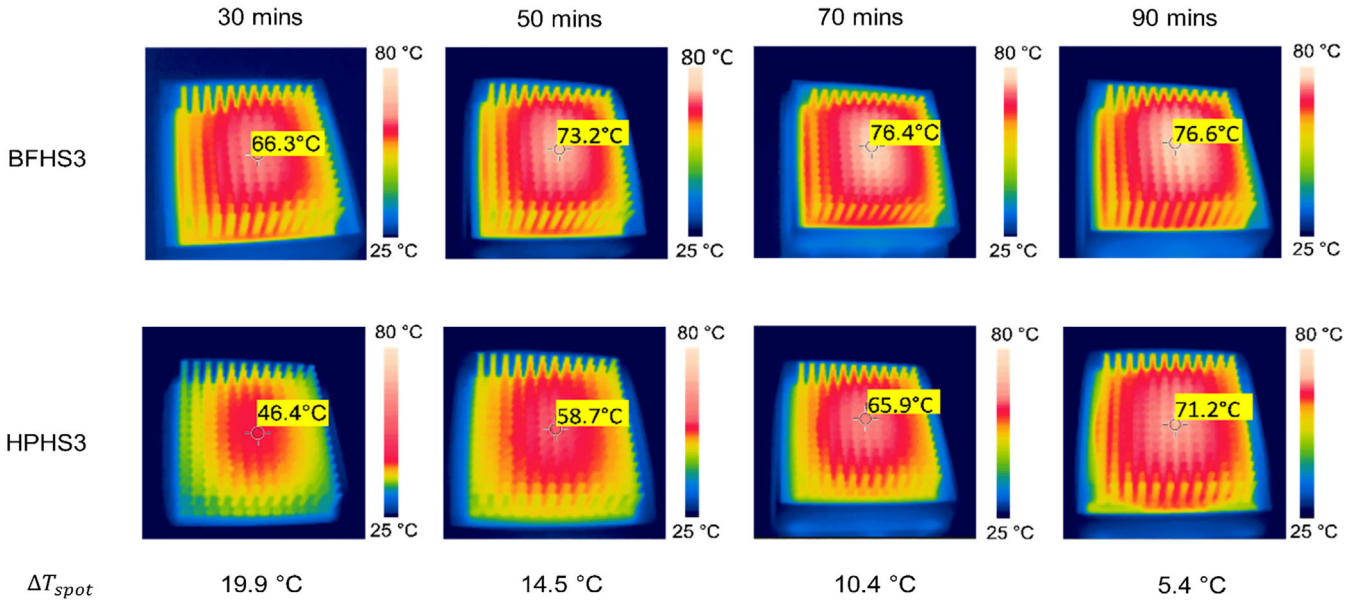

FIGURE 8 A localized hot spot comparison between BFHS3 and HPHS3 at a volume fraction of 0.4 (m_{PCM} = 585 g) and a thermal load of 80 W [Colour figure can be viewed at wileyonlinelibrary.com]

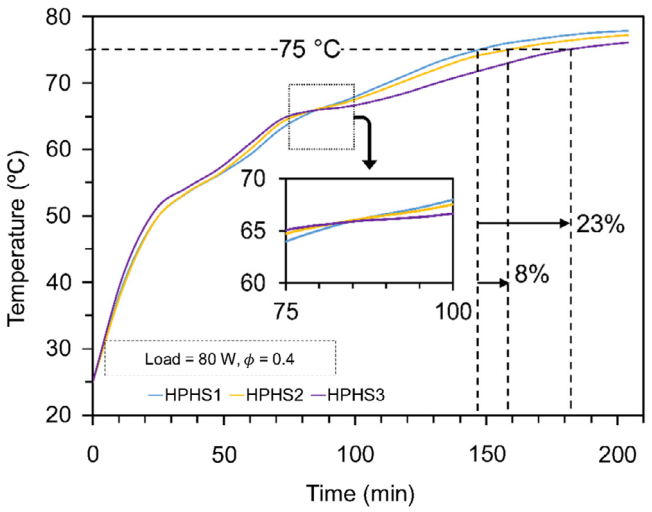

FIGURE 9 Variation in the base temperature profiles for HPHS1, HPHS2, and HPHS3 at a thermal load of 80 W and a PCM volume fraction of 0.4 (m_{PCM} = 585 g) during the heating process [Colour figure can be viewed at wileyonlinelibrary.com]

latent heating up to 65°C, thus the temperature profiles up to the PCM melting is independent of the type of HPHS fin configuration. Later, as the temperature rises during PCM sensible heating, the profiles for different HPHS vary, and the rise in the temperature profile for HPHS1 is higher than HPHS2 followed by HPHS3. The times taken by HPHS1, HPHS2, and HPHS3 for a 10°C temperature rise from 65°C to 75°C are 67 minutes, 83 minutes, and 107 minutes, respectively. The steady-state temperature of HPHS1, HPHS2, and HPHS3 are 77.8°C, 77.2°C, and 76.5°C, respectively. Due to decrease in the maximum heat sink temperature, the thermal conductance (Equation (2)) of HPHS3 (1.55 W/K) is found to be higher than HPHS1 (G = 1.51 W/K), which indicates a higher thermal performance of HPHS3. Even though the surface area of the fins exposed to the ambient after adding PCM is approximately same for all the HPHS, HPHS3 experiences a better performance. As the air flows past the straight interrupted fins, the interruptions prevent the merger of thermal boundary layers and maintains the thermally developing flow which can cause a higher rate of natural heat transfer.

The performance of the HPHS does not vary significantly in the PCM melting regime by changing the fin configuration. However, based on the liquid-sensible heating regime, the performance of straight interrupted fin-based HPHS (HPHS3) was found to be the optimal followed by pin-fin-based HPHS (HPHS2) and inclined interrupted fin-based HPHS (HPHS1).

3.3.2 | Cooling process

During the cooling process, the heat transfer occurs from the PCM to the heat sink, as well as to the ambient. The PCM solidifies and is cooled until it reaches a steady-state temperature condition close to ambient. The cooling experiment was performed after the heating process with a thermal load of 80 W and was allowed to start from the same initial temperature of 75°C for all the HPHS. The base temperature profile of HPHS1, HPHS2, and HPHS3

with a PCM volume fraction of 0.4 is shown in Figure 10. Prior to the onset of the solidification of the PCM, all the HPHS perform similarly and from this temperature onwards, HPHS3 cools faster than HPHS1, followed by HPHS2. The cooling time taken until the completion of the sensible and latent cooling of the PCM for HPHS1, HPHS2, and HPHS3 was 90, 93, and 79 minutes, respectively, whereas, it took another 111, 137, and 115 minutes to cool to a temperature of 30°C. HPHS3 and HPHS1 cooled faster than HPHS2 by 15% and 7% to reach 30°C. At 100 W, the cooling process for all HPHS was started from the same initial temperature of 85°C. The rate of cooling for HPHS3 and HPHS1 to reach 30°C is faster than HPHS2 by 23% and 11%, respectively. At 120 W, the cooling was started from 95°C, where HPHS3 cooled faster than HPHS2 and HPHS1 by 10% to reach 30°C.

Overall, the HPHS with straight interrupted fins delivered the best performance and provided effective heat sink temperature control during the heating and the cooling processes. This may be attributed to their special fin design features with maximum interruption of boundary layers of air currents surrounding the fin surfaces exposed to the ambient.

3.3.3 | Effect of thermal load on the HPHS temperature profile

The base temperature profile of HPHS1 with a PCM volume fraction of 0.4 at thermal loads of 80 W, 100 W, and 120 W is shown in Figure 11. The PCM melts at a faster rate with an increase in the thermal load due to the higher heat transfer rate from the base to the heat sink. As discussed in the previous section, HPHS3 delivered the best performance followed by HPHS2 and HPHS1 for a thermal load of 80 W. At higher thermal loads of 100 W and 120 W, the shape of the temperature profiles for HPHS1, HPHS2, and HPHS3 is similar to that at 80 W, except that the slopes of the temperature profiles are higher. Even at higher thermal loads, the time until the completion of PCM melting was similar for all HPHS. The temperature profile and time delay for the liquid-sensible heating regime are critical for assessing the performance of HPHS. At a 100 W load, the time delays for HPHS3 and HPHS2 to reach 85°C are higher than HPHS1 by 45% and 7%, respectively. Similarly, at a 120 W load, the time delays for HPHS3 and HPHS2 to reach 95°C are higher than for HPHS1 by 8.5% and 6.5%. Overall, the thermal performance of HPHS3 at all the thermal loads was found to be higher than for HPHS2 and HPHS1.

The HPHS base temperatures rise quickly after the completion of the latent heating phase and achieve higher steady-state temperatures for higher thermal loads. For example, the steady-state temperature of HPHS1 for a thermal load of 120 W was higher than 80 W by ~20°C. The steady-state temperatures of HPHS1, HPHS2, and HPHS3 at all thermal loads (80-120 W) are shown in Figure 12. The steady-state temperatures of HPHS3 were lower than HPHS2 and HPHS1 at all the thermal loads.

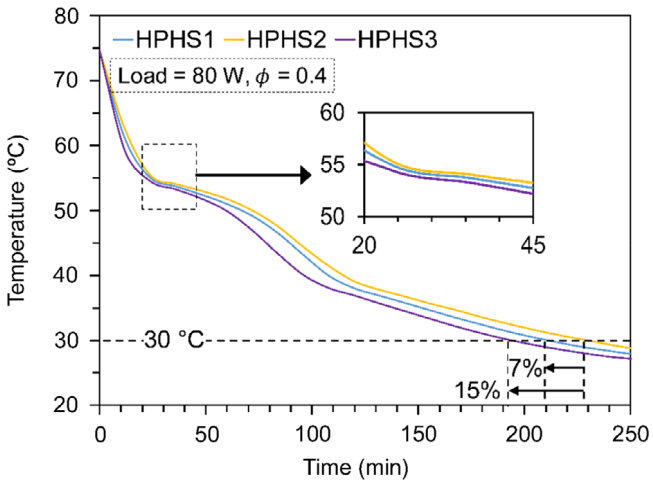

FIGURE 10 Variation in base temperature profile for HPHS1, HPHS2, and HPHS3 for a PCM volume fraction of 0.4 (m_{PCM} = 585 g) during the cooling process [Colour figure can be viewed at wileyonlinelibrary.com]

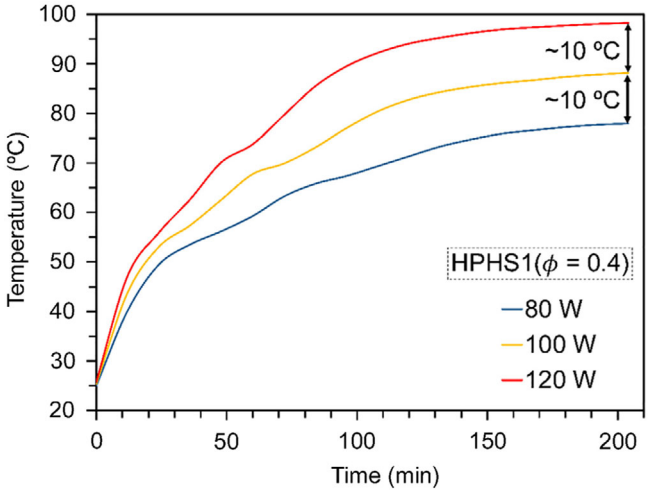

FIGURE 11 Variation in the base temperature profile for HPHS1 with a PCM volume fraction of 0.4 (m_{PCM} = 585 g) at thermal loads of 80 W, 100 W and 120 W [Colour figure can be viewed at wileyonlinelibrary.com]

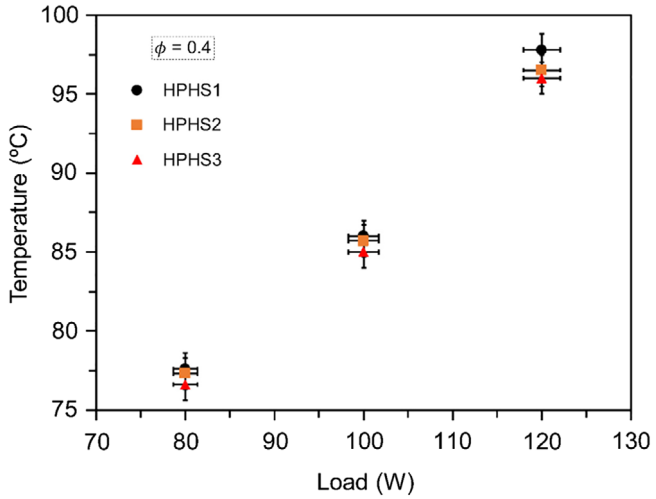

FIGURE 12 Steady-state temperatures achieved by HPHS1, HPHS2, and HPHS3 for thermal loads of 80 W, 100 W, and 120 W [Colour figure can be viewed at wileyonlinelibrary.com]

3.3.4 | Effect of PCM volume fraction on the heat sink performance

With the increase in the quantity of PCM, the storage capacity of the HPHS and the height of the PCM layer increase, whereas, the height of the fins exposed the ambient decreases. The HPHS1 base temperature profiles for a thermal load of 80 W at different volume fractions (ϕ = 0, 0.2, 0.4 and 0.6) are shown in Figure 13A. The PCM mass was increased from 290 g to 825 g for a volume fraction increase from 0.2 to 0.6. It is observed that as the PCM quantity increases, the HPHS temperature profiles have similar shape, however, the PCM melting time increases. The calculated enhancement factor for the volume fractions of 0.2, 0.4, and 0.6 are 2.9, 4, and 4.7, respectively. The enhancement increases by 38% by increasing the volume fraction from 0.2 to 0.4; however, it only increases by 18% by increasing the volume fraction further to 0.6. Therefore, the performance does not improve significantly by increasing the PCM quantity above a threshold. This happens due to the reduction in the fin surfaces exposed to the ambient or due to an increase in the fin surfaces submerged in the PCM. The heat rejection to the ambient reduces, however, the rate of heat transfer to the PCM increases. It is also important to note that as the PCM quantity increases, the energy storage capacity increases, but the overall thermal resistance to heat transfer also increases due to poor thermal conductivity of the PCM. There is a drop in the calculated thermal conductance from 1.55 to 1.42 W/K by increasing the volume fraction from 0.2 to 0.6. Therefore, by adding the PCM in different quantities, there exists a

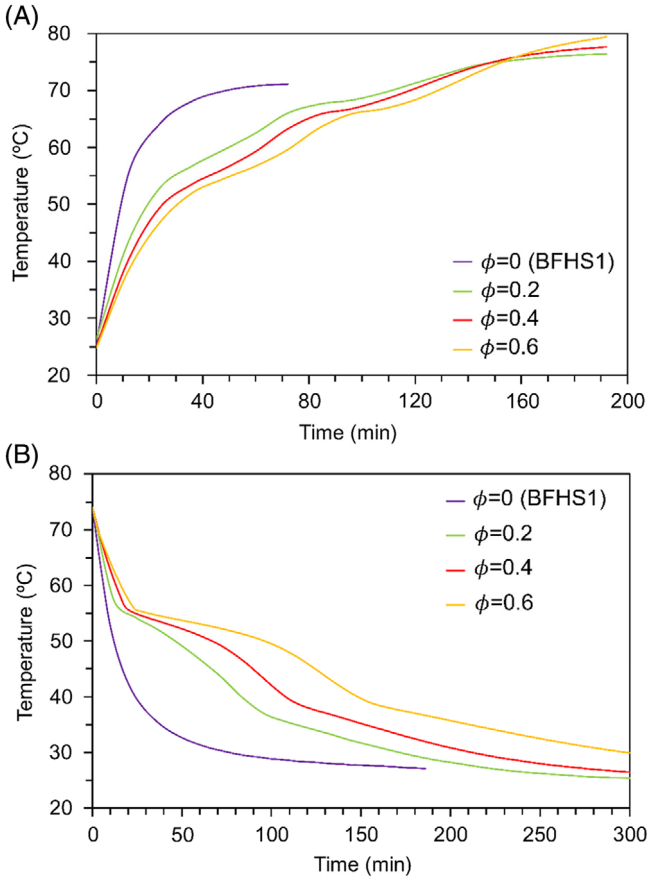

FIGURE 13 Variation in base temperature for HPHS1 for a thermal load of 80 W and different PCM volume fractions (ϕ = 0.2, 0.4, and 0.6) during (A) heating and (B) cooling [Colour figure can be viewed at wileyonlinelibrary.com]

trade-off between the energy storage capacity and the thermal resistance of the PCM.

During the cooling, the heat transfer is only dependent upon the thermal resistance to the heat transfer offered by the PCM. Therefore, higher quantity of PCM results in a lower rate of heat transfer from the heat sink to the ambient. Further, the heat transfer rate drops due to a reduction in fin surfaces exposed to the ambient. This can be observed from the temperature profiles during cooling of HPHS1 with different quantities of the PCM as shown in Figure 13B. Cooling of different PCM volume fractions was started from 75°C. Obviously, the cooling rate is fastest for BFHS1, that is, in the absence of the PCM. HPHS1 with volume fractions of 0.2 and 0.4 cooled faster than that with a volume fraction of 0.6 by 31% and 17% to reach 30°C.

The heating performance of HPHS carrying different quantities of PCM discussed above confers with several previous studies, such as those conducted by Baby and Balaji,[30,31] Ali et al.[25-27] Increasing the PCM quantity leads to an increase in the energy storage capacity and,

hence, high enhancement factors. However, it is important to note that simultaneously, the cooling performance degrades by adding more PCM amount. The improvement in the cooling performance of PCM-based heats sinks has been taken into consideration only recently in the study reported by Akula et al.[35] The HPHS designs discussed in the present study provide some flexibility in choosing the PCM quantity. For example, choosing a lower PCM volume fraction of 0.2 does not affect the heating profile comprehensively, however, the cooling performance is significantly improved. This happens due to a higher active fin volume contributing to the passive cooling mechanism from heat sink to the ambient air.

The illustrations of the heat sink heating can also be understood on the basis of the enhancement factor and thermal conductance values. Figure 14A shows the effect of increasing the PCM quantity on the enhancement factor at different thermal loads of 80 W, 100 W, and 120 W. At different thermal loads, the enhancement factors increased by increasing the PCM volume fraction from 0.4 to 0.6 for all the HPHS. Therefore, the time delay for heat sink temperature rise increases for the range of thermal loads between 80 W and 120 W. The variation in thermal conductance due to an increase in PCM quantity at different thermal loads is plotted in Figure 14B. It is observed that the thermal conductance of the HPHS decreases at all the thermal loads due to increase in the maximum heat sink temperatures. Therefore, by increasing the PCM volume fraction, the storage capacity and the ability to sustain high thermal loads increase, whereas the thermal conductance decreases.

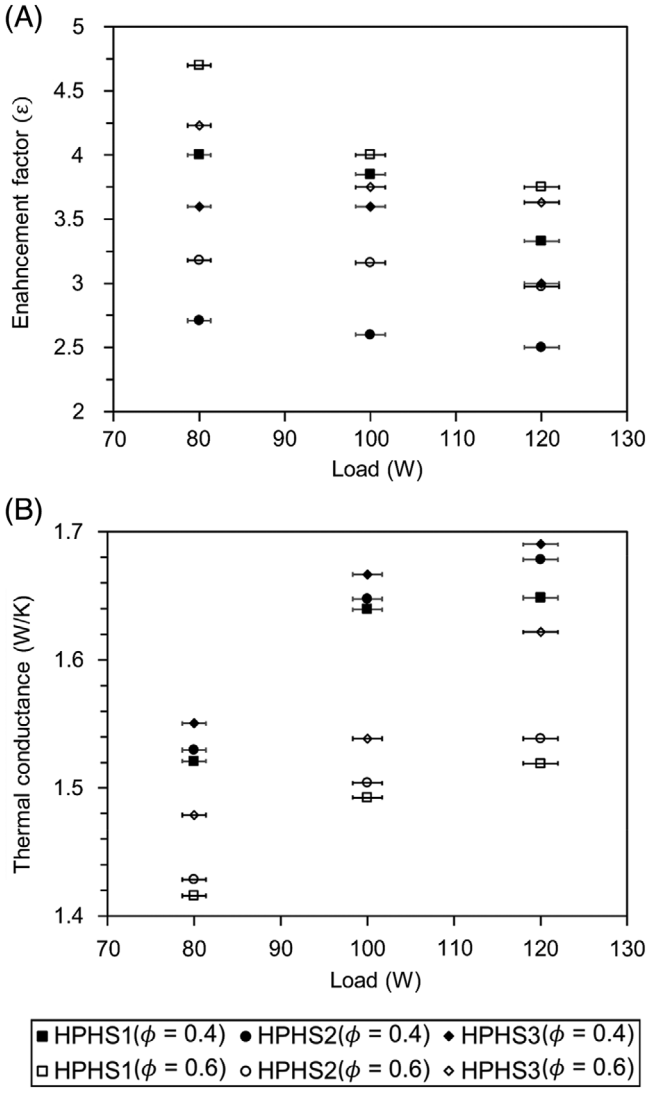

FIGURE 14 (A) Enhancement factor (ε); and (B) thermal conductance (G) for all HPHS (HPHS1, HPHS2, and HPHS3) for volume fractions of 0.4 and 0.6 at different thermal loads (80 W, 100 W, and 120 W)

For the complete range of testing conditions of thermal loads and PCM quantities, the enhancement factors are highest for HPHS1, followed by HPHS3 and HPHS2, as shown in Figure 14A, whereas, the thermal conductance shown in Figure 14B is highest for HPHS3, followed by HPHS2 and HPHS1. As discussed previously, the overall HPHS thermal performance varies based on the liquid-sensible heating regime and maximum heat sink temperature, and therefore, it is optimal for HPHS3. The temperature profiles and the thermal conductance values show that the straight interrupted fins-based HPHS provides the best thermal performance for the complete range of testing conditions. During heating, a higher thermal conductance is observed for all thermal loads and PCM quantities, whereas, during cooling, HPHS3 undergoes fast cooling than the other HPHS. The maximum interruption of the thermal boundary layers in the exposed area of the fins lead to a high rate of heat transfer in straight interrupted fin design than the other designs.

Besides selecting the best HPHS fin configuration and optimum PCM quantity, the heat sink thermal performance depends upon desired operating conditions such as duty-cycle operation, discussed in the next section.

3.4 | Intermittent heat sink thermal loading: Duty cycle operation

With typical device operation, it may be subjected to intermittent loading conditions according to operational duty-cycle requirements. The performances of HPHS and the BFHS were analyzed for three different 50% duty-cycles tests conducted for a range of conditions namely: (a) high load and shorter operation period; (b) intermediate load and operation period; and (c) low load and longer operation period, as follows:

a. Duty cycle A: Thermal load—120 W, ON—30 minutes and OFF—30 minutes, number of heating-cooling cycles (Z) = 4.
b. Duty cycle B: Thermal load—100 W, ON—45 minutes, and OFF—45 minutes, $Z = 4$.
c. Duty cycle C: Thermal load—80 W, ON—60 minutes, and OFF—60 minutes, $Z = 4$.

The PCM temperature variation during the intermittent operation of HPHS1 with a volume fraction of 0.4 (m_{PCM} = 585 g) and BFHS1 for duty cycle A is shown in Figure 15. Initially, during the first heating-cooling cycle, the BFHS approaches steady-state rapidly, whereas, there is a delay in time for the HPHS due to latent heat stored during the melting of PCM. The temperature peak shaving effect caused by the HPHS during the heating process is shown by the area marked in green. During cooling, it is evident that the BFHS drops to a low temperature rapidly as compared to the HPHS due to the absence of PCM thermal resistance. During the next heating-cooling cycle, the BFHS starts from a lower temperature (~38°C) and, therefore, provides some "thermal relaxation" as compared to the HPHS which starts from a higher temperature (~50°C) as shown by area marked in grey. The thermal relaxation is limited as the temperature profile for BFHS matches up rapidly with that for HPHS. This is again followed by the temperature peak shaving effect as the BFHS temperature profile exceeds the HPHS temperature. The peak shaving effect reduces over subsequent cycles due to the slow cooling of the PCM.

The HPHS provides an effective temperature control during the cyclic operation and, hence, reduces the thermal stress on the device during the cyclic operation. The power peak shaving of the HPHS can be evaluated in terms of the energy stored in the PCM (Equation (6)) to the total energy supplied to the heat sink.

$$Q_{stored} = \sum_{Z=1}^{n} \sum_{t=0}^{t_{duty}} \left(m_{PCM} c_{PCM} \left(T_{PCM} - T_{ini} \right) + m_{PCM} L_{ph} f \right), \tag{6}$$

where, c_{PCM}, L_{ph}, and f are the specific heat, latent heat, and melted fraction of PCM (Equation (7)). T_{ini} is the initial temperature before the starting of any heating-cooling cycle. The PCM TMR can be introduced as the ratio of energy stored by the PCM to the energy supplied during a cycle and is shown in Equation (8). The TMRs for the heating-cooling cycles operating at different duty cycles are shown in Figure 16.

$$f = \frac{T_{PCM} - T_{onset}}{T_{end} - T_{onset}}, \tag{7}$$

$$\text{Thermal management ratio} = \frac{Q_{stored}}{Q_{supplied}}. \tag{8}$$

Both the sensible and the latent heating of the PCM lead to higher energy absorbed by the PCM during the first cycle for all the duty cycles. Since the PCM reaches its melting temperature range after the first cycle, the energy is absorbed due to partial melting in the subsequent heating cycles. Hence, the TMR is highest in the first cycle and reduces in the subsequent cycles. It is observed that the HPHS shows a better overall TMR for the duty cycle with a shorter heating process time and

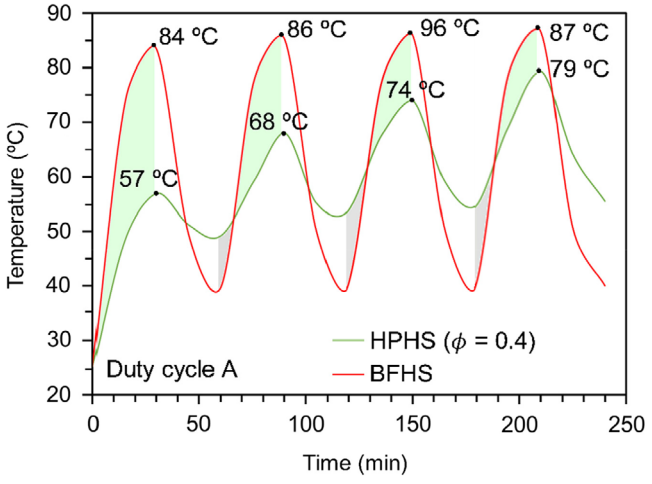

FIGURE 15 Variation in the PCM temperature profile for HPHS1 with a volume fraction of 0.4 (m_{PCM} = 585 g) and BFHS1 for duty cycle A (Thermal load—120 W, ON—30 minutes, and OFF—30 minutes, $Z = 4$) [Colour figure can be viewed at wileyonlinelibrary.com]

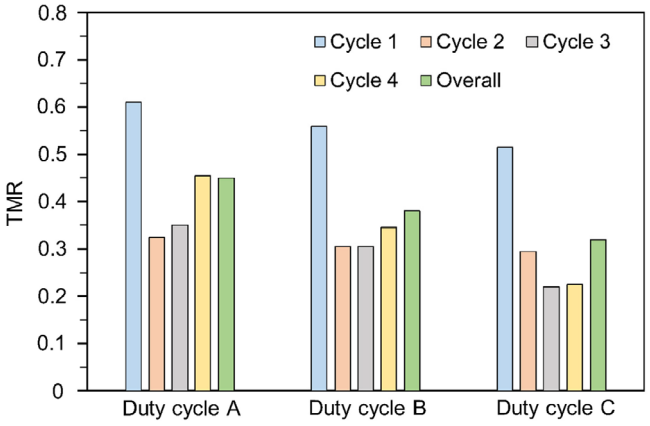

FIGURE 16 Thermal management ratio (TMR) during different heating cycles for duty cycles A, B, and C [Colour figure can be viewed at wileyonlinelibrary.com]

higher thermal load, that is, for duty cycle A. The overall TMR for duty cycle A is 0.45 and is the highest followed by duty cycle B and duty cycle C with TMRs of 0.38 and 0.32, respectively. Therefore, the addition of a PCM layer to BFHS provides substantial power and temperature peak shaving for duty cycle operation.

4 | CONCLUSIONS

In the present study, the HPHS were developed for peak shaving of load in industrial battery chargers (IC650) using paraffin as the PCM. The impact of adding a PCM layer to the BFHS with different fin geometries, namely inclined interrupted fins (HPHS1), pin fins (HPHS2), and straight interrupted fins (HPHS3), was analyzed for different PCM volume fractions and different thermal loads. The heat sinks were subjected to constant (80-120 W) and intermittent thermal loading, and the overall TMR was calculated for the duty cycle operation. The major conclusions from the study are as follows:

- All HPHS provided more effective heat sink temperature control by causing a time delay in heat sink temperature rise than BFHS and extending the operation due to the high energy storage capacity of PCM. The hot spot in the heat sink was cooled by ~5°C to 20°C for a 90 minutes HPHS heating operation.
- The enhancement factor (ε) calculated at the PCM melting temperature was higher for HPHS1 followed by HPHS3 and HPHS2, but the time until the completion of melting was similar for all the HPHS. The overall thermal performance was optimal for HPHS3 based on the liquid-sensible heating regime with lower maximum temperatures and faster rate of cooling.
- Increasing the thermal load on the HPHS from 80 to 120 W led to an increase in steady-state heat sink base temperatures by ~20°C. The steady-state temperatures at all thermal loads were minimal for HPHS3, followed by HPHS2 and HPHS1.
- By increasing the PCM volume fraction from 0.2 to 0.6 during heating, the ε values increased; however, the thermal conductance of the HPHS reduced. The performance during the cooling process deteriorated by increasing the PCM quantity as it increases the heat sink thermal resistance. The optimum PCM quantity required for heat sink hybridization is based on a trade-off between its thermal storage capacity and thermal resistance.
- HPHS is able to provide a non-fluctuating temperature profile and, hence, reduce thermal stresses in heat sinks during a duty-cycle operation. A maximum overall TMR of 0.45 was achieved, and the HPHS operation for a duty cycle with shorter operating period and high load was found to be effective.

ACKNOWLEDGMENTS

The authors are very grateful for the funding of the project, partially sponsored by the "Mathematics of Information Technology and Complex Systems" under the "Mitacs Globalink Research Award" program, and partially by the "Queen Elizabeth Scholars" (QES) under "The Canadian Queen Elizabeth II Diamond Jubilee Scholarships" program. The Canadian Queen Elizabeth II Diamond Jubilee Scholarships (QES) is managed through a unique partnership of Universities Canada, the Rideau Hall Foundation (RHF), Community Foundations of Canada (CFC), and Canadian universities. The QES-AS is made possible with financial support from IDRC and SSHRC. The project was conducted in collaboration with Delta Q Technologies. Their support in terms of data and equipment was highly appreciated. Gurpreet S. Sodhi would also like to thank everyone at the Laboratory for Alternative Energy Conversion (LAEC) for their support and suggestions. The DSC analysis was conducted by Mr. Wen Zhou, Instrument Technician, Department of Chemistry at Simon Fraser University.

NOMENCLATURE

c	specific heat of PCM (J/kg/K)
f	melting fraction
G	thermal conductance (W/K)
H	height of heat sink (m)
I	electric current (A)
k	thermal conductivity (W/m/K)
L	length of heat sink (m)
L_{ph}	latent heat of phase change (J/kg)
m	mass of PCM (kg)
P	power (W)
Q	energy (J)
ΔT_{spot}	temperature difference at the hot spot between the BFHS and HPHS (K)
T	temperature (K)
t	time (s)
V	volume (m^3)
W	width of heat sink (m)
Z	number of cycles

SUBSCRIPTS

a	ambient
f	fusion
ini	initial
m	melting

ABBREVIATIONS

BFHS	bare fin heat sinks
DSC	differential scanning calorimetry
HPHS	hybrid passive heat sinks
PCM	phase change material
TMR	thermal management ratio

DIMENSIONLESS PARAMETERS

$\varepsilon = \frac{t_{HPHS}}{t_{BFHS}}$ enhancement factor

$\phi = \frac{V_{PCM}}{V_{total}}$ volume fraction

DATA AVAILABILITY STATEMENT

Data available on request due to privacy/ethical restrictions.

ORCID

Gurpreet Singh Sodhi https://orcid.org/0000-0001-8713-5490

Muthukumar Palanisamy https://orcid.org/0000-0002-0863-2964

REFERENCES

1. Bunsen T, Cazzola P, D'Amore L, Gorner M, Scheffer S, Schuitmaker R, Signollet H, Tattini J, Paoli JTL. Global EV outlook 2019—scaling up the transition to electric mobility. OECD IeaOrg; 2019:232.
2. Siddique ARM, Mahmud S, Heyst BV. A comprehensive review on a passive (phase change materials) and an active (thermoelectric cooler) battery thermal management system and their limitations. *J Power Sources*. 2018;401:224-237. https://doi.org/10.1016/j.jpowsour.2018.08.094.
3. Ling Z, Zhang Z, Shi G, Fang X, Wang L, Gao X, Fang Y, Xu T, Wang S, Liu X. Review on thermal management systems using phase change materials for electronic components, Li-ion batteries and photovoltaic modules. *Renew Sustain Energy Rev*. 2014;31:427-438. https://doi.org/10.1016/j.rser.2013.12.017.
4. Khattak Z, Ali HM. Air cooled heat sink geometries subjected to forced flow: a critical review. *Int J Heat Mass Transf*. 2019;130:141-161. https://doi.org/10.1016/j.ijheatmasstransfer.2018.08.048.
5. Sohel Murshed SM, Nieto de Castro CA. A critical review of traditional and emerging techniques and fluids for electronics cooling. *Renew Sustain Energy Rev*. 2017;78:821-833. https://doi.org/10.1016/j.rser.2017.04.112.
6. BCC Research. *The Market for Thermal Management Technologies*. Massachusetts, MA: BCC Research LLC; 2019. https://www.bccresearch.com/market-research/semiconductor-manufacturing/market-for-thermal-management-technologies.html.
7. Weng YC, Cho HP, Chang CC, Chen SL. Heat pipe with PCM for electronic cooling. *Appl Energy*. 2011;88:1825-1833. https://doi.org/10.1016/j.apenergy.2010.12.004.
8. Wang JC. U- and L-shaped heat pipes heat sinks for cooling electronic components employed a least square smoothing method. *Microelectron Reliab*. 2014;54:1344-1354. https://doi.org/10.1016/j.microrel.2014.02.034.
9. National Aeronautics and Space Administration. NASA Technology Roadmaps TA14: Thermal Management Systems. NASA Technology Roadmaps; 2015.
10. Hasan MI, Tbena HL. Using of phase change materials to enhance the thermal performance of micro channel heat sink. *Eng Sci Technol*. 2018;21:517-526. https://doi.org/10.1016/j.jestch.2018.03.017.
11. Prajapati YK, Pathak M, Khan MK. Transient heat transfer characteristics of segmented finned microchannels. *Exp Therm Fluid Sci*. 2016;79:134-142. https://doi.org/10.1016/j.expthermflusci.2016.07.004.
12. Jorg J, Taraborrelli S, Sabelberg E, Kneer R, De Doncker R, Rohlfs W. Hot spot removal in power electronics by means of direct liquid jet cooling. *Proc 16th Intersoc Conf Therm Thermomechanical Phenom Electron Syst*. 2017;2017:471-481. https://doi.org/10.1109/ITHERM.2017.7992525.
13. Ianniciello L, Biwolé PH, Achard P. Electric vehicles batteries thermal management systems employing phase change materials. *J Power Sources*. 2018;378:383-403. https://doi.org/10.1016/j.jpowsour.2017.12.071.
14. Kim J, Oh J, Lee H. Review on battery thermal management system for electric vehicles. *Appl Therm Eng*. 2019;149:192-212. https://doi.org/10.1016/j.applthermaleng.2018.12.020.
15. Rao Z, Wang S. A review of power battery thermal energy management. *Renew Sustain Energy Rev*. 2011;15:4554-4571. https://doi.org/10.1016/j.rser.2011.07.096.
16. Yan J, Li K, Chen H, Wang Q, Sun J. Experimental study on the application of phase change material in the dynamic cycling of battery pack system. *Energ Conver Manage*. 2016;128:12-19. https://doi.org/10.1016/j.enconman.2016.09.058.
17. Farzanehnia A, Khatibi M, Sardarabadi M, Passandideh-Fard M. Experimental investigation of multiwall carbon nanotube/paraffin based heat sink for electronic device thermal management. *Energ Conver Manage*. 2019;179:314-325. https://doi.org/10.1016/j.enconman.2018.10.037.
18. Zhou D, Zhao CY. Experimental investigations on heat transfer in phase change materials (PCMs) embedded in porous materials. *Appl Therm Eng*. 2011;31:970-977. https://doi.org/10.1016/j.applthermaleng.2010.11.022.
19. Alshaer WG, Nada SA, Rady MA, Del Barrio EP, Sommier A. Thermal management of electronic devices using carbon foam and PCM/nano-composite. *Int J Therm Sci*. 2015;89:79-86. https://doi.org/10.1016/j.ijthermalsci.2014.10.012.
20. Praveen B, Suresh S, Pethurajan V. Heat transfer performance of graphene nano-platelets laden micro-encapsulated PCM with polymer shell for thermal energy storage based heat sink. *Appl Therm Eng*. 2019;156:237-249. https://doi.org/10.1016/j.applthermaleng.2019.04.072.
21. Kothari R, Mahalkar P, Sahu SK, Kundalwal SI. Experimental investigations on thermal performance of PCM. Proceedings of the ASME 2018 16th International Conference on Nanochannels, Microchannels, and Minichannels ICNMM2018; 2018:1–9.
22. Fan LW, Zhu ZQ, Zeng Y, Xiao YQ, Liu XL, Yu YY, Ding Q, Yu ZT, Cen KF. Transient performance of a PCM-based heat sink with high aspect-ratio carbon nanofillers. *Appl Therm Eng*. 2015;75:532-540. https://doi.org/10.1016/j.applthermaleng.2014.10.050.
23. Ahmadi M, Mostafavi G, Bahrami M. Natural convection from rectangular interrupted fins. *Int J Therm Sci*. 2014;82:62-71. https://doi.org/10.1016/j.ijthermalsci.2014.03.016.

24. Ahmadi M, Pakdaman MF, Bahrami M. Pushing the limits of vertical naturally-cooled heatsinks; calculations and design methodology. *Int J Heat Mass Transf*. 2015;87:11-23. https://doi.org/10.1016/j.ijheatmasstransfer.2015.03.086.
25. Ali HM, Arshad A, Jabbal M, Verdin PG. Thermal management of electronics devices with PCMs filled pin-fin heat sinks: a comparison. *Int J Heat Mass Transf*. 2018;117:1199-1204. https://doi.org/10.1016/j.ijheatmasstransfer.2017.10.065.
26. Ali HM, Ashraf MJ, Giovannelli A, Irfan M, Irshad TB, Hamid HM, Hassan F, Arshad A. Thermal management of electronics: an experimental analysis of triangular, rectangular and circular pin-fin heat sinks for various PCMs. *Int J Heat Mass Transf*. 2018;123:272-284. https://doi.org/10.1016/j.ijheatmasstransfer.2018.02.044.
27. Ali HM, Arshad A. Experimental investigation of n-eicosane based circular pin-fin heat sinks for passive cooling of electronic devices. *Int J Heat Mass Transf*. 2017;112:649-661. https://doi.org/10.1016/j.ijheatmasstransfer.2017.05.004.
28. Mahmoud S, Tang A, Toh C, AL-Dadah R, Soo SL. Experimental investigation of inserts configurations and PCM type on the thermal performance of PCM based heat sinks. *Appl Energy*. 2013;112:1349-1356. https://doi.org/10.1016/j.apenergy.2013.04.059.
29. Fok SC, Shen W, Tan FL. Cooling of portable hand-held electronic devices using phase change materials in finned heat sinks. *Int J Therm Sci*. 2010;49:109-117. https://doi.org/10.1016/j.ijthermalsci.2009.06.011.
30. Baby R, Balaji C. Experimental investigations on phase change material based finned heat sinks for electronic equipment cooling. *Int J Heat Mass Transf*. 2012;55:1642-1649. https://doi.org/10.1016/j.ijheatmasstransfer.2011.11.020.
31. Baby R, Balaji C. Thermal optimization of PCM based pin fin heat sinks: an experimental study. *Appl Therm Eng*. 2013;54:65-77. https://doi.org/10.1016/j.applthermaleng.2012.10.056.
32. Jaworski M. Thermal performance of heat spreader for electronics cooling with incorporated phase change material. *Appl Therm Eng*. 2012;35:212-219. https://doi.org/10.1016/j.applthermaleng.2011.10.036.
33. Wang Q, Zhou D, Chen Y, Eames P, Wu Z. Characterization and effects of thermal cycling on the properties of paraffin/expanded graphite composites. *Renew Energy*. 2020;147:1131-1138. https://doi.org/10.1016/j.renene.2019.09.091.
34. Zarma I, Ahmed M. Thermal management of concentrator photovoltaic systems using nano-enhanced phase change materials-based heat sink. *Int J Energy Res*. 2020;44:7713-7733. https://doi.org/10.1002/er.5504.
35. Akula R, Gopinath A, Rangarajan S, Balaji C. Experimental and numerical studies on heat transfer from a PCM based heat sink with baffles. *Int J Therm Sci*. 2021;106525:159. https://doi.org/10.1016/j.ijthermalsci.2020.106525.
36. Kozak Y, Abramzon B, Ziskind G. Experimental and numerical investigation of a hybrid PCM-air heat sink. *Appl Therm Eng*. 2013;59:142-152. https://doi.org/10.1016/j.applthermaleng.2013.05.021.
37. Taghilou M, Khavasi E. Thermal behavior of a PCM filled heat sink: the contrast between ambient heat convection and heat thermal storage. *Appl Therm Eng*. 2020;174:115273. https://doi.org/10.1016/j.applthermaleng.2020.115273.
38. Ghanbarpour A, Hosseini MJ, Ranjbar AA, Rahimi M, Bahrampoury R, Ghanbarpour M. Evaluation of heat sink performance using PCM and vapor chamber/heat pipe. *Renew Energy*. 2021;163:698-719. https://doi.org/10.1016/j.renene.2020.08.154.
39. Kandasamy R, Wang XQ, Mujumdar AS. Application of phase change materials in thermal management of electronics. *Appl Therm Eng*. 2007;27:2822-2832. https://doi.org/10.1016/j.applthermaleng.2006.12.013.
40. Wu W, Zhang G, Ke X, Yang X, Wang Z, Liu C. Preparation and thermal conductivity enhancement of composite phase change materials for electronic thermal management. *Energ Conver Manage*. 2015;101:278-284. https://doi.org/10.1016/j.enconman.2015.05.050.
41. Baby R, Balaji C. Thermal performance of a PCM heat sink under different heat loads: an experimental study. *Int J Therm Sci*. 2014;79:240-249. https://doi.org/10.1016/j.ijthermalsci.2013.12.018.
42. Krishna J, Kishore PS, Solomon AB. Heat pipe with nano enhanced-PCM for electronic cooling application. *Exp Therm Fluid Sci*. 2017;81:84-92. https://doi.org/10.1016/j.expthermflusci.2016.10.014.
43. Zhang Z, Lau E, Botting C, Bahrami M. Naturally cooled heat sinks for battery chargers. *Int J Heat Mass Transf*. 2020;147:118911. https://doi.org/10.1016/j.ijheatmasstransfer.2019.118911.
44. Delta Q Technologies. IC 650 2013. https://delta-q.com/product/ic650-industrial-battery-charger
45. Arshad A, Ali HM, Khushnood S, Jabbal M. Experimental investigation of PCM based round pin-fin heat sinks for thermal management of electronics: effect of pin-fin diameter. *Int J Heat Mass Transf*. 2018;117:861-872. https://doi.org/10.1016/j.ijheatmasstransfer.2017.10.008.
46. Gharbi S, Harmand S, Ben JS. Experimental comparison between different configurations of PCM based heat sinks for cooling electronic components. *Appl Therm Eng*. 2015;87:454-462. https://doi.org/10.1016/j.applthermaleng.2015.05.024.
47. Holman JP. *Experimental Methods for Engineers*. 8th ed. New York, NY: McGraw-Hill; 2001.
48. Fujii M. Enhancement of natural convection heat transfer from a vertical heated plate using inclined fins. *Heat Transfer*. 2007;36:334-344. https://doi.org/10.1002/htj.20168.
49. Kraus A, Aziz A, Welty J, Sekulic D. Extended surface heat transfer. *Appl Mech Rev*. 2001;54:B92. https://doi.org/10.1115/1.1399680.
50. Zhang Z. Passive Cooling System: An Integrated Solution to the Application in Power Electronics (Doctoral dissertation, Applied Sciences: School of Mechatronic Systems Engineering). 2019.
51. Fayazmanesh K, McCague C, Bahrami M. Consolidated adsorbent containing graphite flakes for heat-driven water sorption cooling systems. *Appl Therm Eng*. 2017;123:753-760. https://doi.org/10.1016/j.applthermaleng.2017.05.114.

How to cite this article: Sodhi GS, Botting C, Lau E, Palanisamy M, Rouhani M, Bahrami M. Hybrid heat sinks for thermal management of passively cooled battery chargers. *Int J Energy Res*. 2021;45:6333–6349. https://doi.org/10.1002/er.6260

APPENDIX A.

Selection of PCM for the heat sink testing

For the selection of a suitable PCM for heat sink testing, the findings from a numerical model of a preliminary heat sink prototype developed by the authors have been discussed here. The base temperature distribution of a pin fin–based heat sink with thermal load 100 W and PCM volume fraction 0.4, and with added PCMs namely RT 35, PCM 58, and RT 82, is shown Figure A1. The PCMs used are commercial industrial grade paraffin wax with nearly identical properties but having melting temperatures of 35°C (RT 35), 58°C (PCM 58), and 82°C (RT 82).

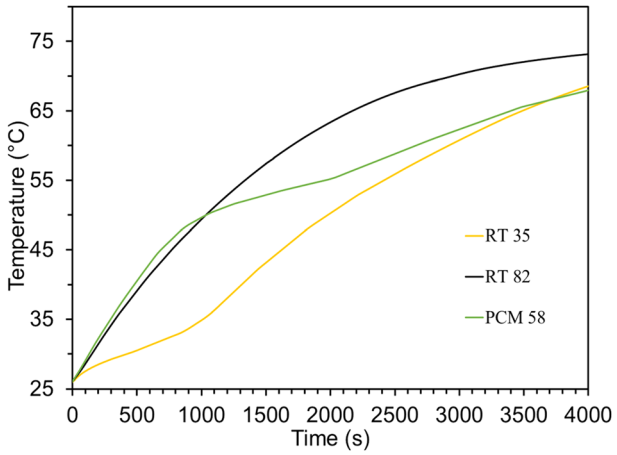

FIGURE A1 Heat sink base temperature profile for different commercial PCMs (paraffin waxes) namely RT 35, PCM 58, and RT 82 [Colour figure can be viewed at wileyonlinelibrary.com]

The PCM is selected based on the following conditions;

i. Utilization of the latent heat potential of the PCM: It is observed from Figure A1 that for a fixed thermal load (100 W in this case) and PCM quantity (volume fraction of 0.4 in this case), both the RT 35 and PCM 58 melt completely. Therefore, the latent heat is completely absorbed by these PCMs. RT 82 on the other hand undergoes sensible heating, whereas, the latent heating is incomplete, which forfeits the purpose of using the PCM.
ii. During the melting phase, PCMs with melting temperature 35°C and 58°C maintain the base temperature below the desired maximum device operating temperature and, hence, the device will operate safely. The utilization of PCMs is justified in their melting temperature range.
However, while cooling from a fixed maximum temperature, the solidification behavior of both RT35 and PCM 58 will be different. Since, the ambient temperature is fixed, the temperature difference between the solidification temperature and the ambient is higher for PCM 58 than RT 35 due to which, solidification occurs at a faster rate in case of PCM 58. Therefore, restoration of the device for starting a fresh heating (device ON mode) process will be quick for PCM 58.

The PCM selected for the HPHS in the present study is intended to extend the isothermal battery charger operation near the melting point temperature and absorb the latent heat completely. Hence, the selection of PCM 58 is justified for the overall heating-cooling operation.